JIPB Journal of Integrative Plant Biology

Research Article
https://doi.org/10.1111/jipb.70387

The miR168a–*TaAGO1b* module improves *Fusarium* head blight resistance and yield in wheat

Guoliang Chen[1,2†], Shuaifeng Geng[1,3†], Zhongyin Deng[1†], Yuqing Che[1†], Ziying Wang[1], Tianhua Chen[1,3], Dada Cui[1], Xinyu Zou[1], Qihang Chen[1], Wanxin Xu[1], Zixu Zhao[1], Ziyi Yan[1], Tingting Li[2], Zili Ye[1], Jiajie Wu[4], Xigang Liu[5], Min Zhang[2*], Long Mao[1,3*], Aili Li[1*] and Shaoshuai Liu[1,3*]

1. State Key Laboratory of Crop Gene Resources and Breeding and National Key Facility for Crop Resources and Genetic Improvement, Institute of Crop Sciences, Chinese Academy of Agricultural Sciences, Beijing 100081, China
2. College of Agronomy, Sichuan Agricultural University, Chengdu 611130, China
3. National Center of Technology Innovation for Comprehensive Utilization of Saline-Alkali Land, Dongying, Shandong 257000, China
4. State Key Laboratory of Wheat Improvement, College of Agronomy, Shandong Agricultural University, Tai'an 271018, China
5. Ministry of Education Key Laboratory of Molecular and Cellular Biology, College of Life Sciences, Hebei Normal University, Shijiazhuang 050024, China

†These authors contributed equally to this work.

*Correspondences: Shaoshuai Liu (liushaoshuai@caas.cn, Dr. Liu is fully responsible for the distribution of all materials associated with this article); Min Zhang (yalanmin@126.com); Long Mao (maolong@caas.cn); Aili Li (liaili@caas.cn)

Guoliang Chen

Shaoshuai Liu

ABSTRACT

Fusarium head blight (FHB) is a devastating fungal disease of wheat that causes severe yield loss and mycotoxin contamination. Wheat varieties offering higher grain yield while maintaining moderate resistance to FHB are highly desirable. Here, we report that microRNA168a (miR168a) acts as a key negative regulator of both FHB resistance and grain yield in wheat. Knockdown of miR168a via target mimicry (MIM168) enhanced resistance to FHB in transgenic plants, accompanied by increased H_2O_2 accumulation and restricted fungal spread. MIM168 plants also exhibited higher grain yield with longer spikes and higher spikelet number per spike under uninfected field conditions. By contrast, miR168a overexpression (OE168) lines became more susceptible to FHB and displayed significantly reduced grain yield. We further identified *TaAGO1b* as a target of miR168a. Knockout of *TaAGO1b* using CRISPR/Cas9 (*ago1b*) recapitulated the FHB susceptibility and reduced spike length, demonstrating that miR168a and *TaAGO1b* work as a module. Moreover, miR168a positively regulates the miR156–*TaSPL17* module, which is associated with spike development, and it also regulates miR444 in FHB infection, and that knockdown of miR444 via target mimicry (MIM444) enhances FHB resistance. Meanwhile, *ago1b* mutations upregulated miR156 and miR444. Thus, our data demonstrated that the miR168a–*TaAGO1b* module contributes to wheat spike architecture and FHB resistance via miR156 and miR444, providing a potential strategy for breeding high-yielding and FHB-resistant wheat varieties.

Keywords: AGO1b, *Fusarium* head blight, miR168a, miR444, wheat

Chen, G., Geng, S., Deng, Z., Che, Y., Wang, Z., Chen, T., Cui, D., Zou, X., Chen, Q., Xu, W., et al. (2026). The miR168a–*TaAGO1b* module improves *Fusarium* head blight resistance and yield in wheat. J. Integr. Plant Biol. **00:** 1–16.

INTRODUCTION

Common wheat (*Triticum aestivum*) is one of the most important crops in the world, providing calories for about 40% of the global population. Wheat production, however, is severely threatened by various diseases that compromise global food security. *Fusarium* head blight (FHB) is a devastating fungal disease of wheat, primarily caused by *Fusarium*

graminearum, leading to significant yield losses and mycotoxin (e.g., deoxynivalenol, DON) contamination (Alisaac and Mahlein, 2023; Liu et al., 2025). Cultivating FHB-resistant wheat varieties represents an effective and sustainable strategy for disease management. More than 642 quantitative trait loci (QTLs) associated with FHB resistance have been identified in wheat (Shang et al., 2024; Song et al., 2024; Viviani et al., 2025; Ning et al., 2026). FHB resistance is a complex quantitative trait governed by combined effects of multiple loci with minor contributions. Among these, a few major-effect genes, such as *Fhb1* and *Fhb7*, have been extensively characterized and widely utilized in breeding programs (Li et al., 2019, 2023; Su et al., 2019; Wang et al., 2020). Investigating novel FHB-resistance genes is crucial for providing a theoretical basis for breeding strategies aimed at improving wheat resistance.

Crop resistance to disease requires energy that often causes yield loss, or so-called trade-offs, highlighting the complexity of optimizing the two traits (Karasov et al., 2017). Despite these challenges, recent progress has shown that immunity can be enhanced without incurring yield penalties. A wheat resistance gene, *Tamlo-R32*, for instance, is capable of maintaining growth and yield while providing strong resistance to powdery mildew (Li et al., 2022a). Another example is the CRISPR/Cas9-mediated knockout of *TaMKP1*, which enhanced wheat resistance against rust and powdery mildew with greater yield (Liu et al., 2024). In addition, the wheat E3 ubiquitin ligase TaHAKAI degrades the viral RNA silencing suppressor P2, thereby inhibiting viral infection, but increasing spike length and spikelet number in wheat (Guo et al., 2025). More recently, overexpression of *TaPIP2;10* increased grain yield and enhanced wheat resistance to FHB and other biotic stresses (Lu et al., 2022). These studies suggest that resistance and yield improvement can be simultaneously achieved, although such cases remain limited. Therefore, identifying key regulatory hubs that coordinate these competing pathways is critical.

At the regulatory level, microRNAs (miRNAs) have emerged as critical small noncoding RNAs (20–24 nt) that regulate plant development and immunity (Chen, 2009; Attallah et al., 2025; Fahad et al., 2025; Yu et al., 2026; Guo et al., 2026). Among them, the miR168 family participates in diverse biological processes, including plant growth and development (Xian et al., 2014; Zhou et al., 2020; Zhou et al., 2022). miR168 also participates in plant responses to abiotic stress (Liu et al., 2020) and biotic stress (viruses and fungi) (Várallyay et al., 2010; Iki et al., 2018; Wang et al., 2021; Feng et al., 2023). ARGONAUTE 1 (AGO1) is the core component of the RNA-induced silencing complex (RISC). It mediates miRNA-guided gene silencing in plants (Zhang et al., 2015). AGO1 is a conserved target of miR168, forming a feedback loop that maintains small RNA homeostasis (Xian et al., 2014; Zhao et al., 2026). As the primary effector of most miRNAs, AGO1 regulation can influence multiple downstream pathways (Morel et al., 2002; Carbonell, 2017; Lopez-Gomollon and Baulcombe, 2022). Functional diversification of *AGO1* homologs has been reported in plants, with AGO1 associating with endogenous small RNAs to establish a complex regulatory network that targets a broad repertoire of downstream genes related to growth, development, and stress responses (Kapoor et al., 2008; Li et al., 2022b; Zhao et al., 2023). However, whether miR168-mediated regulation of AGO1 exhibits functional specialization in hexaploid wheat remains unclear. More importantly, whether the miR168–AGO1 module can coordinately regulate yield and disease resistance, especially FHB in wheat, remains unknown.

Here, we report that miR168a and *TaAGO1b* work as a module in wheat. Knockdown of miR168a enhances resistance to FHB and increases grain yield in field trials, whereas knockout of *TaAGO1b*, a target of miR168a, by CRISPR/Cas9 caused increased FHB susceptibility and shortened spike length. Further analysis reveals that the miR168a–*TaAGO1b* module regulates spike architecture and immunity through the downstream miR156- and miR444-mediated regulatory pathways. Our work thus demonstrates that manipulating a single miRNA can simultaneously improve multiple important agronomic traits, highlighting the potential strategy to breed wheat varieties with higher yield and enhanced disease resistance.

RESULTS

Knockdown of miR168a enhances wheat resistance to FHB

Plant miRNAs are global regulators of gene expression that control plant growth, development, and immunity (Shen et al., 2024; Yu et al., 2026). We examined miRNAs that have the potential to modulate wheat immunity, growth, and yield. Genome-wide analysis identified three *MIR168a* loci located on chromosomes 6A, 6B, and 6D in wheat (Figures 1A, S1A). To investigate the biological function of miR168a, we generated transgenic lines overexpressing miR168a (OE168) or suppressing miR168a using a target mimicry strategy (MIM168) in the wheat cultivar Fielder (Figure 1B). OE168 lines displayed significantly elevated miR168a levels, whereas MIM168 lines showed reduced levels in the T_2 generation relative to those in WT (Figure 1C).

First, to examine the role of miR168a in regulating FHB, we conducted single-floret point inoculation on florets at anthesis. MIM168 plants showed markedly fewer symptomatic spikelets at 14 d post inoculation (dpi) (Figure 1D, E) and accumulated significantly less fungal biomass compared with WT plants (Figure 1F), whereas OE168-1 and OE168-2 plants developed more symptomatic spikelets. Further field inoculation across two spring seasons in 2025 and 2026 demonstrated that MIM168 rendered weaker FHB symptoms, whereas OE168-1 and OE168-2 increased FHB susceptibility in transgenic plants (Figure 1G, H). Moreover, MIM168 plants exhibited a markedly lower proportion of FHB-infected grains and reduced yield loss under disease conditions compared with those of WT plants (Figure 1I, J). Consistent with these disease symptoms, DON accumulation

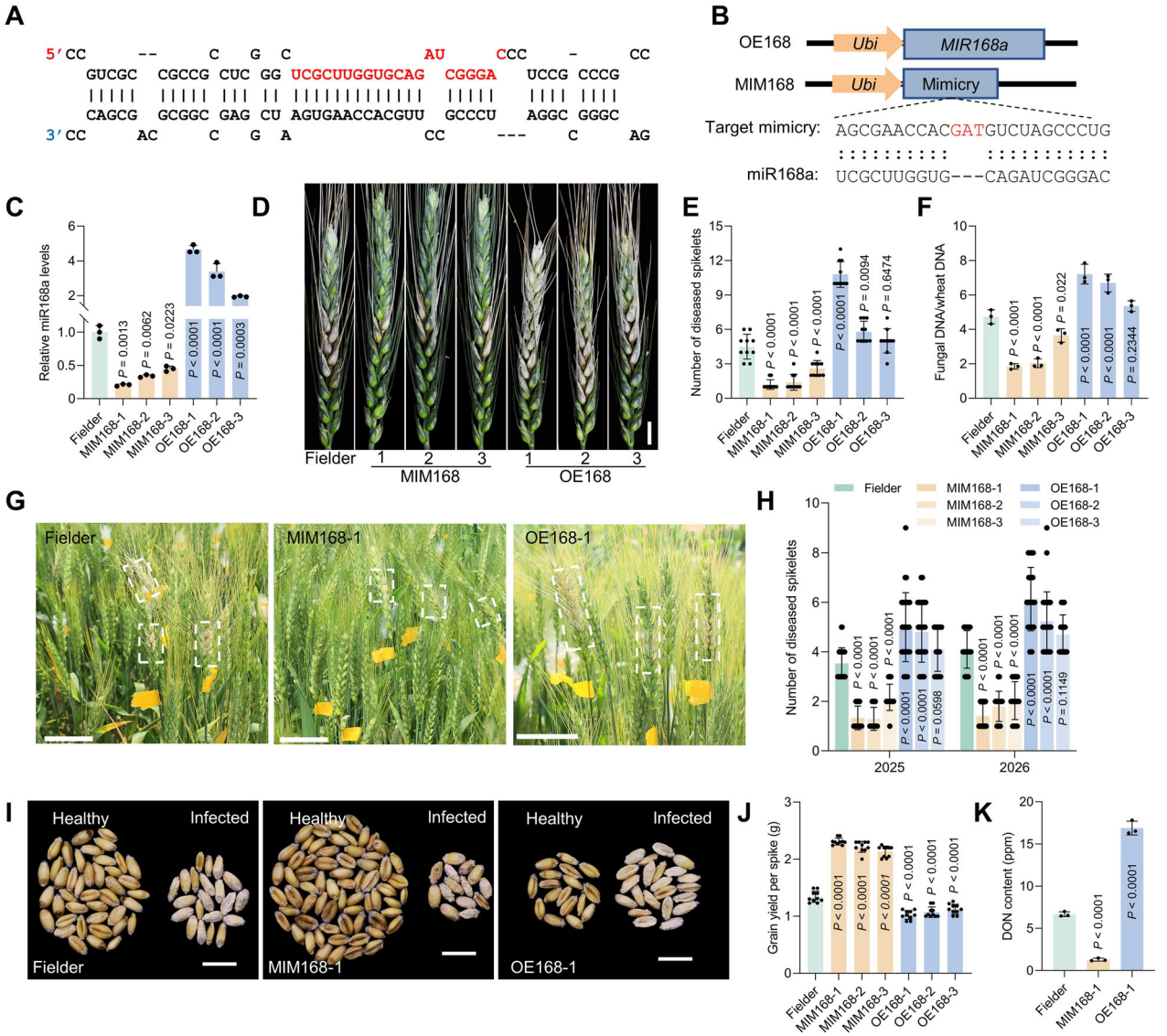

Figure 1. miR168a modulates wheat immunity to FHB

(A) Secondary structure of the *MIR168a* precursor from chromosome 6A in wheat. Red sequences indicate mature miR168a-5p. **(B)** Schematic diagrams of the OE168 and MIM168 transgenic constructs. The OE168 construct contains the miR168a precursor flanked by 300 bp of upstream and downstream genomic sequences. The MIM168 construct expresses a target mimic of miR168a to inhibit its activity. **(C)** RT-qPCR analysis of miR168a abundance in three independent T_2 lines of OE168 and MIM168. **(D)** Representative images of FHB symptoms on transgenic wheat spikes at 14 dpi in the greenhouse. Scale bars, 1 cm. **(E)** Statistical analysis of the number of diseased spikelets on main spikes of wheat plants ($n = 10$) in the greenhouse. **(F)** Quantification of relative fungal biomass in infected spikelets from main spikes of plants grown in the greenhouse ($n = 5$). Five spikelets, one each from five main spikes of five independent plants, were pooled as one biological sample for DNA extraction and RT-qPCR analysis. **(G)** Disease symptoms on representative spikes at 14 dpi of FHB inoculation of transgenic plants and the control in the field. Scale bars, 5 cm. **(H)** Quantification of diseased spikelets on inoculated main spikes ($n = 30$) under field conditions in 2025 and 2026. **(I)** Representative images of diseased and healthy grains from Fielder, MIM168, and OE168 lines following FHB inoculation in the field. Scale bar, 1 cm. **(J)** Grain yield per main spike ($n = 10$) following *F. graminearum* inoculation under field conditions. **(K)** Suppression of miR168a reduces DON accumulation in infected grains. *P* values were determined by one-way analysis of variance (ANOVA). All values are means ± *SD* and three independent biological replicates were performed.

in infected grains was significantly lower in MIM168 plants than that in Fielder, whereas OE168 plants showed significantly higher DON accumulation than Fielder (Figure 1K).

Confocal microscopy analysis of GFP-labeled *F. graminearum* revealed that hyphal progression was markedly restricted in MIM168 tissues from 24 hpi to 72 hpi, but extended in OE168 plants (Figure 2A, B). To elucidate the mechanisms underlying disease resistance, we monitored the production of reactive oxygen species (ROS) bursts after inoculation. MIM168 plants accumulated significantly higher levels of H_2O_2 at 24 and 48 h post-inoculation (hpi), whereas OE168 plants exhibited reduced H_2O_2 accumulation relative to that of WT (Figure 2C, D). RT-qPCR analysis showed that both *TaPR1* and *TaPR5* were strongly induced in MIM168 spikelets but remained at relatively low levels in those of OE168 following *F. graminearum* infection, whereas no

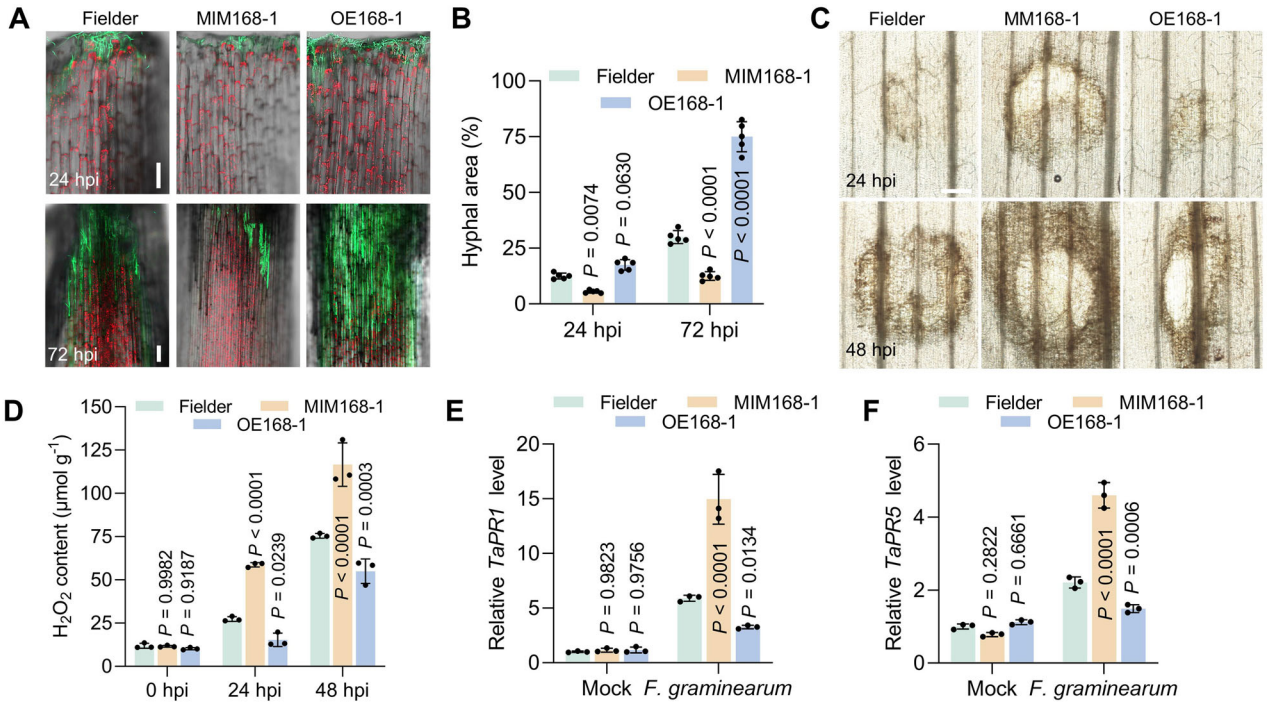

Figure 2. miR168a suppresses H_2O_2 accumulation and promotes fungal infection progression

(A) Microscopic observation of peeled wheat coleoptiles inoculated with a GFP-tagged PH-1 strain at indicated time points. The coleoptiles exhibited autofluorescence of chloroplasts (red) in mesophyll cells and that of the plant cell wall. Scale bars, 100 μm. **(B)** Quantification of fluorescent hyphal area in wheat coleoptiles ($n = 5$). **(C)** Representative images of DAB staining showing H_2O_2 accumulation in leaves of Fielder, MIM168, and OE168 at 24 and 48 hpi. Dark brown precipitates indicate the presence of H_2O_2. Scale bar, 200 μm. **(D)** Quantification of H_2O_2 content in spikelets of Fielder, MIM168, and OE168 at 0, 24, and 48 hpi after *F. graminearum* inoculation. Spikelets from five spikes were pooled for each biological replicate. **(E, F)** RT-qPCR analysis of *TaPR1* **(E)** and *TaPR5* **(F)** expression levels in spikelets of Fielder, MIM168, and OE168 at 48 hpi following *F. graminearum* inoculation or mock treatment. *P* values were determined by ANOVA. All values are means ± *SD* and three independent biological replicates were performed.

significant differences were observed among genotypes treated with mock solution (Figure 2E, F). These results demonstrate that miR168a knockdown enhances wheat resistance to FHB with reduced DON accumulation in infected grains, consistent with increased ROS accumulation and elevated expression of downstream defense-related genes.

miR168a knockdown enhances grain yield by increasing spikelet number per spike

Increasing disease resistance often reduces plant yield, due to the growth-defense trade-off (He et al., 2022). We then explored yield-related traits for transgenic lines. We found that MIM168 plants displayed a significantly increased spike length compared with that of WT, whereas the spike length of OE168 plants was reduced (Figure 3A, C). Consistent with the increased spike length, MIM168 rachises developed significantly more internodes (Figure 3B), increasing their spikelet number per spike (SPS) (Figure 3D). Conversely, OE168 plants showed opposite phenotypes, including fewer internodes and SPS. To investigate the developmental basis of this distinct spike morphology, we examined W3-stage inflorescences from greenhouse-grown plants using scanning electron microscopy (SEM) (Waddington et al., 1983). This analysis revealed that MIM168 spikes initiated a significantly higher number of spikelet primordia compared with those of WT (Figure S2A). These results indicated that miR168a influenced spikelet primordium initiation at early developmental stages, thereby shaping the final spike architecture. MIM168 lines also produced significantly higher grain number per spike (GNS) than that of WT under greenhouse conditions (Figure S2B, D). Although grain number per spike increased in MIM168 plants, the grain size was smaller, with reduced length and thousand-grain weight (TGW) compared with that of WT (Figure S2C, E–G). Taken together, these results indicated that miR168a regulates spike architecture and grain number in wheat.

To evaluate whether miR168a confers a yield-enhancing advantage, we conducted comprehensive field assessments at the experimental station in Shunyi, Beijing, across two spring seasons in 2025 and 2026. Compared with WT and OE168, MIM168 plants exhibited significantly longer spikes (Figures 3E, S3A) and higher grain number per spike under field conditions (Figure 3G). Consistent with these traits, grain yield per 50 plants was significantly higher for MIM168 lines than that of the wild type in the two growing seasons (Figure 3H). Although MIM168 plants produced a higher number of grains, significantly reduced TGW was observed in MIM168-1 and MIM168-2 (Figure 3I). Further phenotypic

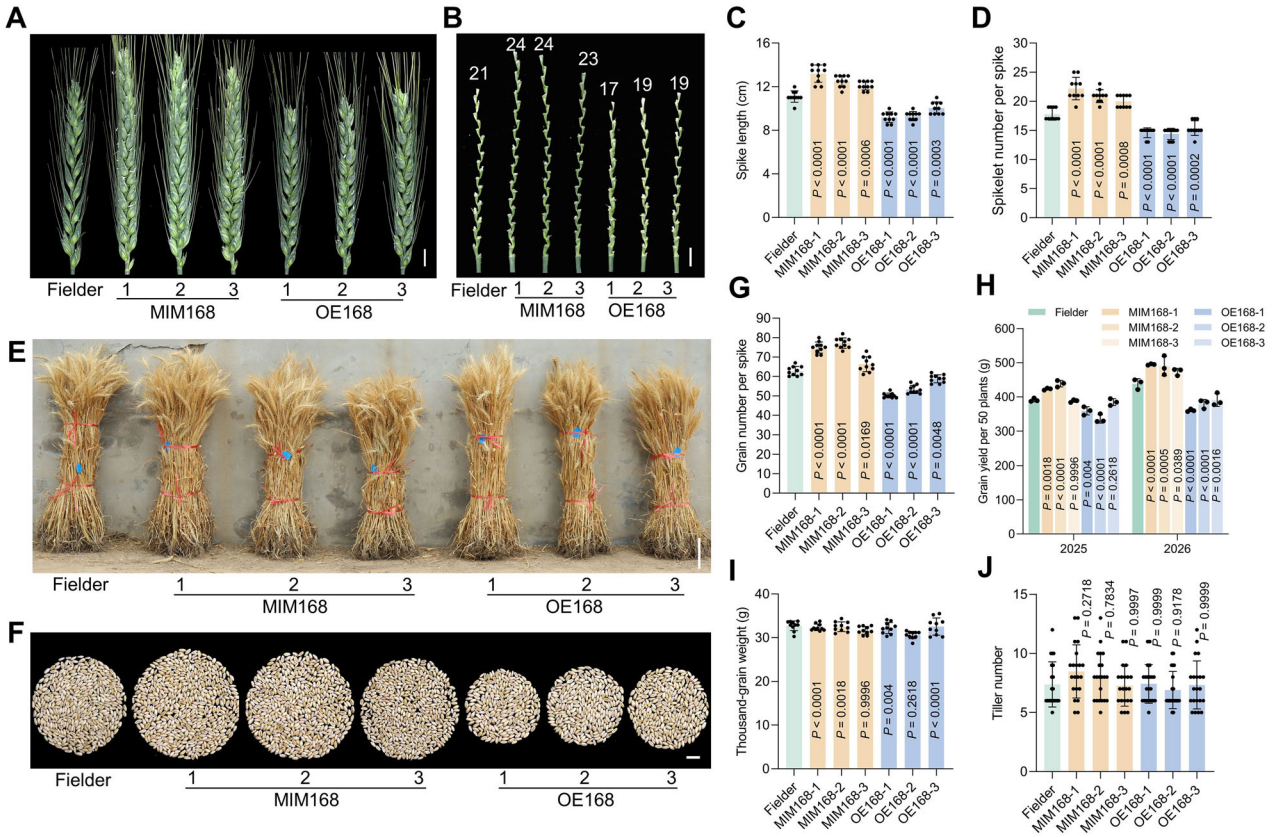

Figure 3. miR168a negatively regulates grain yield

(A) Spike morphology of wheat lines as indicated. Scale bars, 1 cm. **(B)** Rachis internode number analysis. Scale bars, 1 cm. **(C, D)** Statistical analysis of spike length **(C)** and spikelet number per spike **(D)** ($n = 10$). **(E)** Field phenotypic observations of Fielder, MIM168, and OE168 plants. Scale bars, 10 cm. **(F)** Grain number per plant. Scale bars, 1 cm. **(G–J)** Statistical analysis of yield-related traits under field conditions ($n = 10$). Grain number per spike **(G)**, grain yield per 50 plants **(H)**, TGW ($n = 10$) **(I)**, and tiller number ($n = 20$ plants) **(J)**. *P* values were determined by ANOVA. All values are means ± *SD* and three independent biological replicates were performed.

observation found that MIM168 plants exhibited reduced grain length (Figure S3B, C) but increased grain width in MIM168-1 and MIM168-2 (Figure S3D). Beyond spike and grain traits, the number of tillers appeared to be increased in MIM168 plants, though not statistically significant (Figure 3J). Together, these results indicated that knockdown of miR168a enhances wheat yield in the field primarily by increasing GNS.

miR168a targets *TaAGO1b* to regulate FHB resistance and spike morphology

Previous studies have established *AGO1*s as central effectors of the miRNA pathway and a conserved target of miR168a in plants (Vaucheret et al., 2004). Sequence alignment of wheat *AGO1* family members revealed that the miR168a binding sites are highly conserved, with only minor nucleotide variations among different homoeologs (Table S6; Figure S4A). Tissue-specific expression profiling further showed that *TaAGO1b*, *TaAGO1c*, and *TaAGO1d* are preferentially expressed in spikes, whereas *TaAGO1a* is predominantly expressed in roots (Figure S4B). Given that *AGO1d* plays a specialized role in reproductive phasiRNA pathways and fertility in grasses, we focused subsequent analyses on *TaAGO1b* and *TaAGO1c* to explore the miR168a–*AGO1* regulatory module in spike development and disease response.

To assess the effects of altered miR168a levels, we examined *TaAGO1b* and *TaAGO1c* expression in WT, MIM168, and OE168 lines. RT-qPCR analysis showed that *TaAGO1b* expression was significantly upregulated in spikelets of MIM168 plants but downregulated in those of OE168 lines from W3.5 stage to anthesis (Figures S5A, 4A). In contrast, *TaAGO1c* showed no expression level changes in both transgenic plants (Figure S6A, B). To examine how the miR168a–*TaAGO1b* module responds to pathogen infection, we performed time-course RT-qPCR analysis and found that miR168a accumulation was significantly reduced from 24 to 72 hpi following *F. graminearum* inoculation (Figure S1B). Interestingly, transcript levels of all three *TaAGO1b* homoeologs were reduced after infection (Figures S5B–D). To test whether *TaAGO1b* and *TaAGO1c* are directly regulated by miR168a, we performed 5′-RLM-RACE and transient reporter assays. Cleavage products corresponding to miR168a-mediated slicing were detected for all three *TaAGO1b* homoeologs at the canonical tenth nucleotide of the target site, whereas no cleavage products were detected for

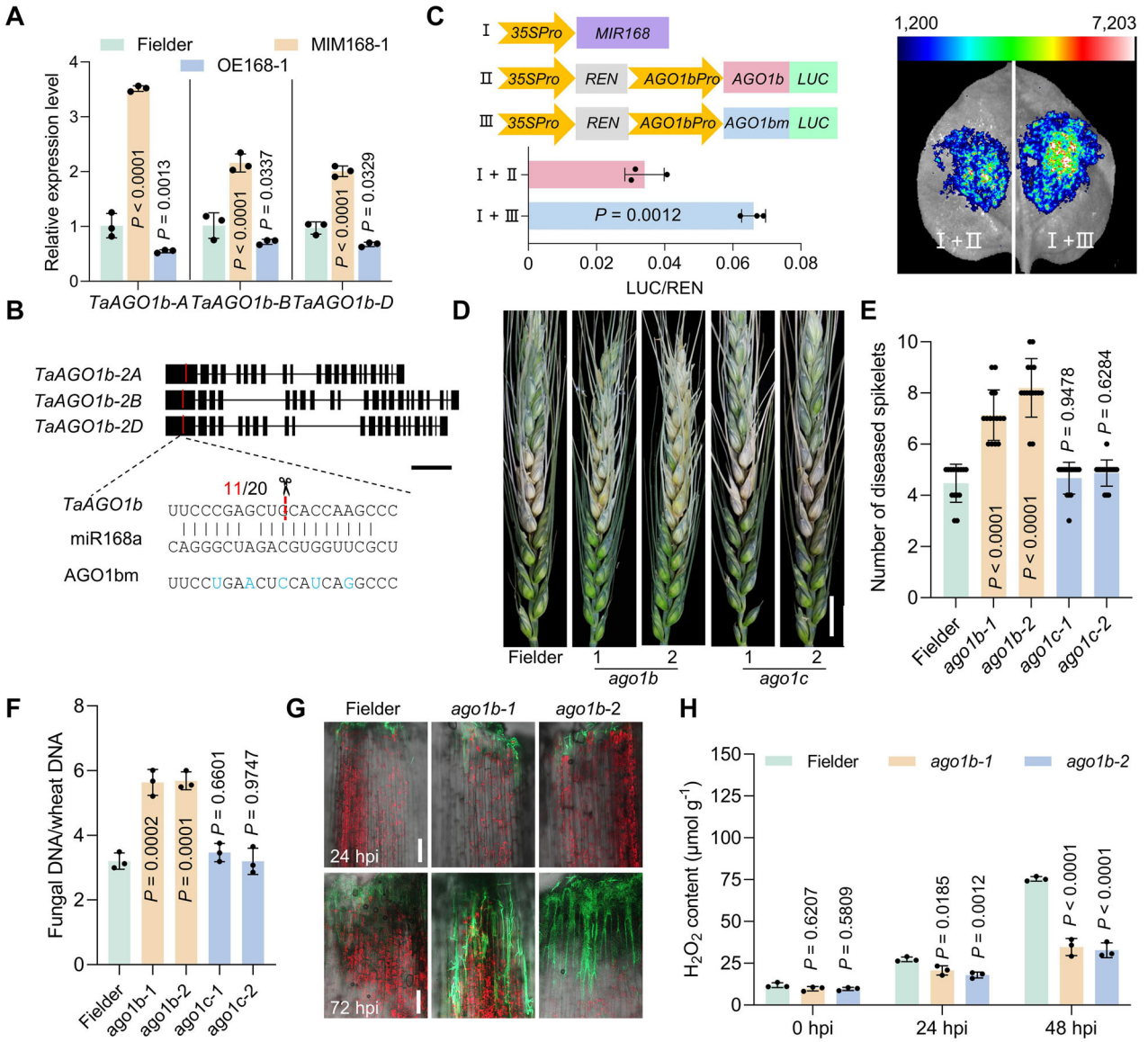

Figure 4. miR168a targets *TaAGO1b* to regulate FHB resistance

(A) RT-qPCR analysis of *TaAGO1b* expression in spikes of WT, MIM168, and OE168 plants at anthesis. **(B)** 5′-RLM-RACE analysis for *TaAGO1b* mRNA cleavage at the canonical miR168a target site. Frequency of the sequenced 5′ ends and alignments of miR168a with target sites in the *TaAGO1b* coding sequence (CDS) and the mutant CDS (AGO1bm) were shown below the gene structure. Scale bar, 1 kb. **(C)** Validation of *TaAGO1b* as a miR168a target through transient expression analysis in *N. benthamiana* leaves. Left: Constructs in *Agrobacterium tumefaciens*. Middle: Representative photograph of firefly luciferase fluorescence signals. Right: Relative reporter activity of indicated construct combinations. **(D)** Representative images of FHB symptoms on Fielder, *ago1b*, and *ago1c* mutants at 14 dpi following *F. graminearum* inoculation. Scale bar, 1 cm. **(E)** Statistical analysis of the number of diseased spikelets on the main spike of wheat plants ($n = 10$) in the greenhouse. **(F)** Quantification of relative fungal biomass in infected spikelets from main spikes of plants grown in the greenhouse. DNA extracted from five independent spikelets (one per spike) was pooled for qPCR analysis. **(G)** Microscopic observation of peeled wheat coleoptiles inoculated with the GFP-tagged PH-1 strain at indicated time points. The coleoptiles exhibited autofluorescence of chloroplasts (red) in mesophyll cells and that of the plant cell wall. Scale bar, 100 μm. **(H)** Quantification of H_2O_2 content in spikelets of Fielder and *ago1b* mutants at 0, 24, and 48 hpi following *F. graminearum* inoculation. Spikelets from five spikes were pooled for each biological replicate. *P* values were determined by ANOVA. All values are means ± *SD* and three independent biological replicates were performed.

TaAGO1c (Figure 4B). Consistently, dual-luciferase reporter assays showed that the LUC/REN activity was significantly lower when pre-miR168a transcripts were co-expressed with the *TaAGO1b* target site compared with those with mutated target sites (Figure 4C). In contrast, no significant repression was observed for the *TaAGO1c* target site (Figure S6C).

To functionally dissect the roles of *TaAGO1b* and *TaAGO1c* in spike morphology and disease response, we generated independent CRISPR/Cas9 knockout lines for both genes in the Fielder background. Homozygous T_3 mutant plants with editing events in all homoeologs were obtained for both *ago1b* and *ago1c* (Figure S7A, B). We first

assessed the response of these mutants to fungal infection. We found that, following single-floret point inoculation with *F. graminearum* at anthesis, *ago1b* mutants exhibited increased susceptibility, as evidenced by significantly more diseased spikelets (Figure 4D, E) and higher fungal biomass at 14 dpi compared with that of WT plants (Figure 4F). In contrast, *ago1c* mutants showed disease symptoms like those of WT plants, with no significant differences in disease severity or fungal growth. Microscopic analysis further revealed enhanced hyphal proliferation in *ago1b* mutants at 24 hpi and 72 hpi (Figure 4G). In addition, pathogen-induced H_2O_2 accumulation was markedly reduced in *ago1b* mutants relative to that in WT plants (Figure 4H), a pattern consistent with that observed in OE168 plants.

In addition to immune defects, we examined whether these mutations also affect plant development. Phenotypic analysis showed that *ago1b* mutants exhibited pronounced defects in spike morphology, including significantly reduced spike length (Figure S8A), fewer SPS (Figure S8B), and a reduced GNS (Figure S8C, D). Furthermore, the *ago1b* mutants showed increased TGW (Figure S8F) and grain length (Figure S8G), with no significant change in grain width (Figure S8H), while grain yield per 50 plants was significantly reduced (Figure S8E). In contrast, *ago1c* mutants exhibited normal spike architecture indistinguishable from WT plants and showed no significant differences in yield-related traits. Collectively, these results indicated that *TaAGO1b* acts as a target of miR168a-mediated regulation and that the miR168a–*TaAGO1b* module controlled both FHB resistance and spike architectural traits in wheat.

The miR168a–*TaAGO1b* module determines spike morphology through miR156

To characterize miRNA co-expression patterns regulating spike development, we performed sRNA-seq on W3.5-stage spikes of Fielder, MIM168, and OE168 plants. In total, 111 expressed miRNAs were identified and grouped into four clusters (C1–C4) (Figure S9A; Table S2). Notably, miRNAs in C1 encompass key developmental regulators, such as miR156 and miR171, which were significantly upregulated in OE168 plants but downregulated in MIM168 plants (Figure 5A). GO enrichment analysis indicated that the predicted targets of C1 miRNAs were mainly involved in cell differentiation and auxin-related signaling pathways (Figure S9A; Table S3).

We then performed RNA-seq on spikes of the same stage (Figure S10A). Compared with the control Fielder, MIM168 plants showed 886 upregulated and 1,701 downregulated genes, whereas OE168 plants showed 1,520 upregulated and 874 downregulated genes (Figures 5B, S10B). GO enrichment of DEGs showed that genes related to flowering regulation and photosynthesis were specifically enriched among upregulated genes in MIM168 (Figure S10C). By overlapping the predicted targets of C1 miRNAs with DEGs identified in both transgenic lines, we obtained 12 candidate genes potentially regulated by C1 miRNAs (Figure 5C). Among these, *TaSPL17* has been reported to positively regulate grain number by regulating spikelet and floret meristem development, and *TaSPL17* overexpression increases grain yield per plant through enhanced grain number and grain size (Liu et al., 2023). In our work, expression analysis showed that *TaSPL17* homoeologs (*7A* and *7D*) exhibited opposite expression patterns to those of C1 miRNAs, with increased transcript abundance in MIM168 plants and reduced levels in OE168 plants (Figure 5D). To validate the relationship between miR156 and *TaSPL17*, we performed stem-loop RT-qPCR assays and found that miR156 levels were significantly elevated in OE168 plants but reduced in MIM168 plants (Figure 5F), whereas *TaSPL17* transcripts showed opposite trends (Figure 5E). To verify direct cleavage of *TaSPL17* mRNA by miR156, we performed 5′-RLM-RACE, and sequencing of amplified products revealed cleavage at the canonical position between the 10th and 11th nucleotides within the miR156 complementary region (Figure 5G). Consistently, dual-luciferase reporter assays showed that co-expression of miR156 with the wild-type *TaSPL17* target sequence significantly reduced luciferase activity, whereas mutation of the miR156 binding site abolished this repression (Figure 5H). To further test whether miR156 is affected by *TaAGO1b*, we examined the abundance of mature miR156 and its precursor transcripts in *ago1b* mutants and found that both were accumulated to higher levels in the mutants than in WT plants (Figure S9B, C). Thus, our findings demonstrate that the miR168a–*TaAGO1b* module is involved in regulating miR156-*TaSPL17*-based spike development.

The miR168a–*TaAGO1b* module mediates FHB resistance through miR444

To investigate how the miR168a–*TaAGO1b* module regulates downstream miRNA pathways and contributes to the development of FHB resistance, integrated small RNA-sequencing (sRNA-seq) and RNA-sequencing (RNA-seq) analysis were conducted on wheat spikelets at anthesis that were inoculated with FHB. We identified 129 miRNAs that can be categorized into eight co-expression clusters (Table S4). As shown in Figure 6A, Cluster 1 (C1) exhibited specific induction in OE168 upon infection, whereas C7 was significantly induced in MIM168. Crucially, C5 was downregulated in both WT and MIM168, with the lowest expression levels observed in MIM168. GO enrichment analysis revealed that C5 cluster targets are highly enriched in defense signaling pathways, such as “MAP kinase kinase kinase activity” and “stess-activated protein kinase signaling cascade” (Figure 6A; Table S5). These findings indicated that C5 was crucial in regulating wheat resistance to FHB.

To determine how the altered miRNA landscape impacts the expression of downstream target genes, we conducted transcriptome profiling of spikelets at 48 hpi (Figure S11A). While *F. graminearum* infection triggered widespread transcriptional changes in Fielder, the magnitude of this response was genotype-dependent. OE168 plants displayed a drastic transcriptomic shift, with the number of DEGs being nearly threefold higher than that in MIM168 plants (Figure S11B).

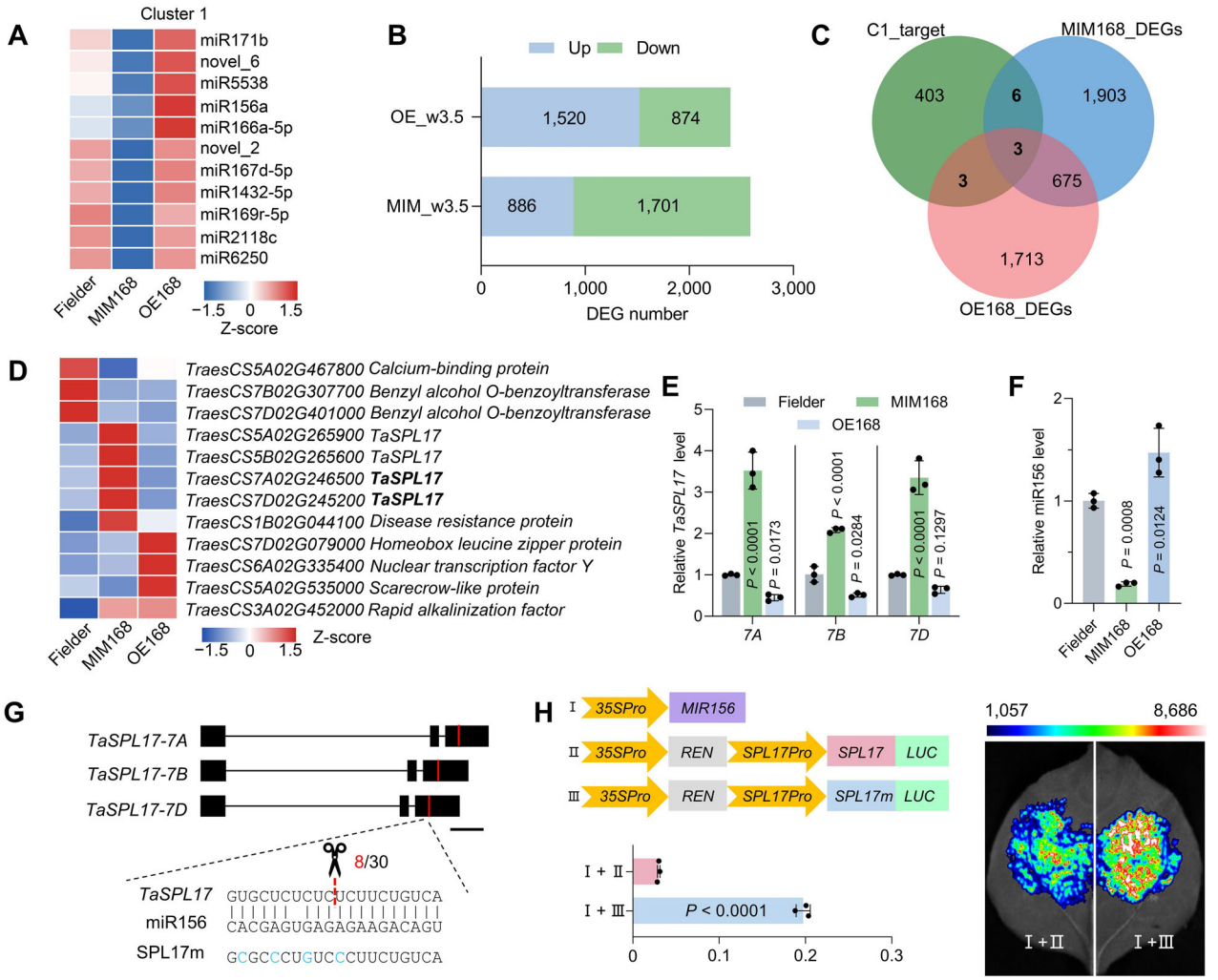

Figure 5. miR168a positively regulates the miR156–*TaSPL17* module for spike development

(A) Heatmap showing the expression patterns of representative miRNAs in Cluster 1 (C1). **(B)** Number of DEGs in MIM168 and OE168 plants relative to Fielder at the W3.5 stage. **(C)** Venn diagram showing the overlap between predicted targets of C1 miRNAs and DEGs identified at the W3.5 stage. **(D)** Heatmap showing expression levels of the 12 genes overlapping with C1 miRNA targets at the W3.5 stage. **(E, F)** RT-qPCR validation of *TaSPL17* homoeologs **(E)** and miR156 **(F)** expression in spikes of the indicated genotypes at the W3.5 stage. **(G)** 5′-RLM-RACE analysis confirming the miR156-directed cleavage site on the *TaSPL17* mRNA. The arrow indicates the cleavage position, and the frequency of cleavage events detected in sequenced clones is shown (8/30). Scale bar, 500 bp. **(H)** Validation of *TaSPL17* as a target of miR156 using a dual-luciferase reporter assay in *N. benthamiana* leaves. *P* values in **(E)** and **(F)** were determined by one-way ANOVA, and in **(H)** by two-tailed Student's *t*-test. All values are means ± *SD* and three independent biological replicates were performed.

GO enrichment analysis revealed that genes specifically upregulated in MIM168 after FHB infection were significantly enriched in ROS-related biological processes (Figure S11C, D). To identify core functional targets within the miR168–*TaAGO1b*–miRNA network, we overlapped the predicted targets of C5 miRNAs with the total DEGs, resulting in a subset of 352 genes (Figure 6B). Expression analysis of these candidates revealed clear genotype-dependent changes in transcript abundance in response to FHB inoculation. Among them, six miRNAs belonged to the C5 cluster. The expression patterns of several representative genes across different genotypes showed an inverse trend with their corresponding miRNAs, consistent with the expectation of miRNA-mediated suppression (Figure 6C). To assess direct responsiveness of these six miRNAs to FHB, we performed stem-loop RT-qPCR to quantify their expression after inoculation. The abundance of miR444 was elevated by FHB infection in OE168 plants, whereas this induction was markedly attenuated in Fielder and MIM168 plants (Figure 6D). We further investigated whether *TaAGO1b* affected miR444 abundance. RT-qPCR analysis revealed that both mature miR444 and its precursor transcripts accumulated to significantly higher levels in *ago1b* mutants than those in wild-type plants (Figure S11E, F), indicating that loss of function of *TaAGO1b* promoted the accumulation of miR444 precursors and mature miR444. These results further indicate that miR444 acts downstream of *TaAGO1b*.

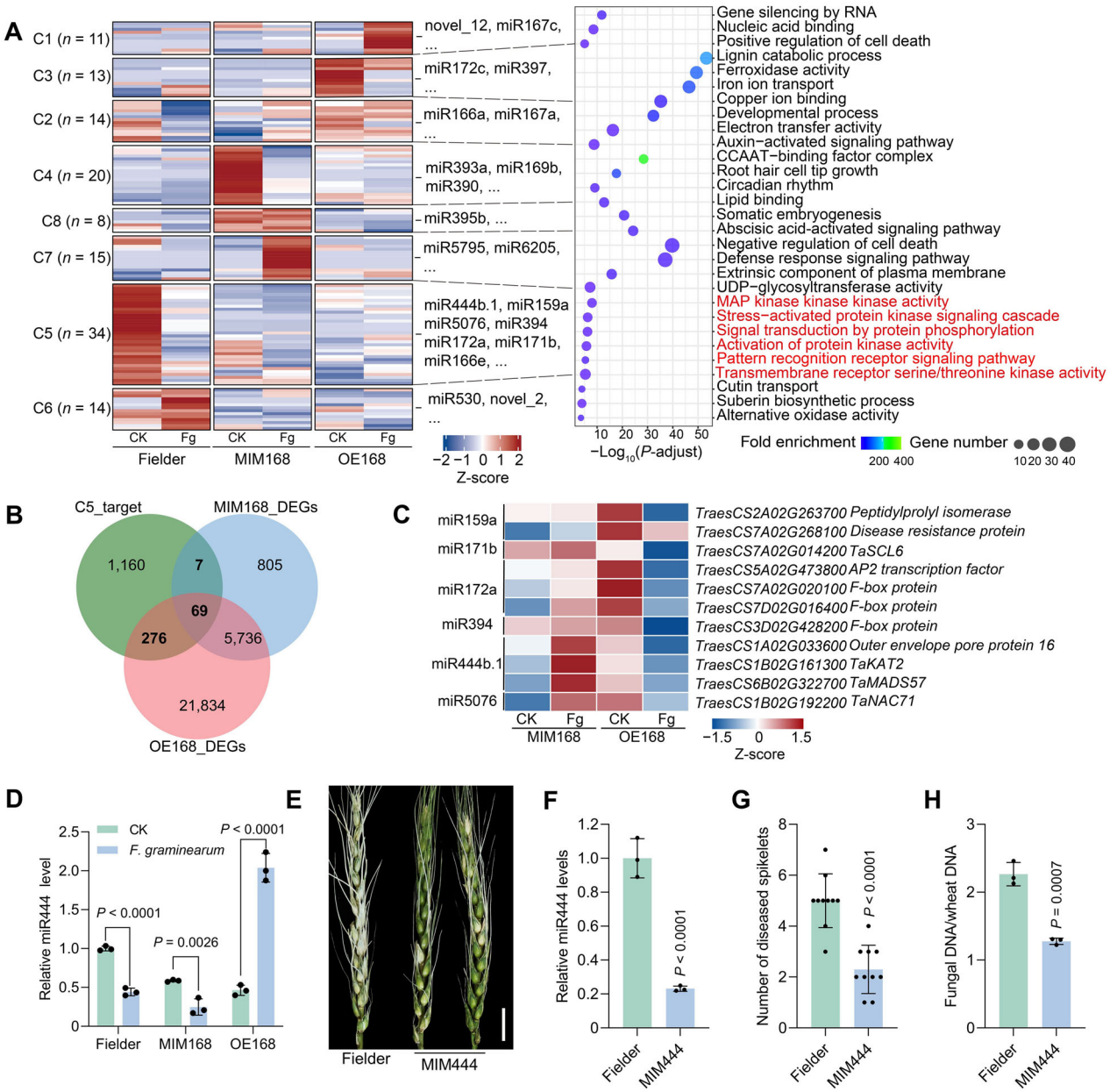

Figure 6. miR444 is involved in regulating FHB resistance in the miR168a–*TaAGO1b* regulatory network

(A) Heatmap illustrating the eight clusters of all miRNAs identified by *K*-means clustering in Fielder, MIM168, and OE168 plants at 48 hpi. Numbers on the left are miRNA counts. The dashed boxes in the middle highlight representative miRNAs, and the right side shows functional enrichment for target genes of each miRNA module (C1–C8) (two-sided Fisher's exact test, Benjamini–Hochberg for multiple comparisons, *P*-adjust < 0.05. The bubble size corresponds to the number of genes annotated to a given term, and the color scale represents fold enrichment). **(B)** Venn diagram showing the overlap between predicted targets of C5 miRNAs and DEGs identified in MIM168 and OE168 plants at 48 hpi relative to mocks. **(C)** Heatmap of representative overlapping genes from **(B)** in MIM168 and OE168 plants upon FHB infection. **(D)** RT-qPCR validation of miR444 expression in Fielder, MIM168, and OE168 plants. **(E)** Disease symptoms of WT and MIM444 T_0 transgenic wheat spikes at 14 dpi with *F. graminearum*. Scale bar, 1 cm. **(F)** RT-qPCR analysis of miR444 accumulation in Fielder and two independent MIM444 transgenic lines. **(G)** Number of diseased spikelets in WT and MIM444 plants at 14 dpi. **(H)** Relative fungal biomass was determined by quantifying fungal DNA relative to wheat DNA. *P* values were determined by one-way ANOVA. All values are means ± *SD* and three independent biological replicates were performed.

We then generated miR444-silenced transgenic wheat lines in the Fielder background using an STTM-based target mimic strategy (MIM444). RT-qPCR confirmed that miR444 accumulation was significantly reduced in two independent MIM444 lines compared with that in the wild type (Figure 6F). Following point inoculation with FHB, the MIM444 lines displayed reduced disease symptoms, fewer diseased spikelets at 14 dpi (Figure 6E, G), and significantly lower fungal biomass than those in the wild type (Figure 6H). These spike-based results were consistent with the enhanced resistance observed following BSMV-mediated silencing of miR444 (Figure S12). Together, these results demonstrate

that miR444 functions as a negative regulator of wheat immunity against FHB.

DISCUSSION

Exploring regulators of disease tolerance that do not incur growth penalties provides an effective strategy for crop genetic improvement. miRNAs are global gene regulators involved in plant growth, development, and immunity (Tang and Chu, 2017; Yu et al., 2026). In this study, we produced miR168a knockdown and overexpression mutants in wheat and investigated their functions in immunity and yield. Our results showed that MIM168 lines exhibit enhanced resistance to FHB, accompanied by increased ROS accumulation. Consistently, genes associated with the GO term "oxalate oxidase activity", a ROS-generating pathway, were enriched among MIM168-specific upregulated genes after infection (Table S7). Importantly, miR168a determines spike morphology. Knockdown of miR168a increases spike length and grain number per plant and significantly increases grain yield. Together, our data indicate that miR168a acts as a key regulator for yield and disease resistance in wheat.

miR168 is conserved and has been implicated as a critical regulator by regulating its exclusive target *AGO1* (Vaucheret et al., 2006). *AGO1* works as an executor component of the RISC and is considered to be a key component in miRNA pathways (Vaucheret et al., 2004). Moreover, miRNA activity can be reshaped through modulation of *AGO* expression and localization, as well as competition for miRNA duplex loading under diverse challenges (Annacondia and Martinez, 2021). Here, we demonstrated that *TaAGO1b*, instead of *TaAGO1c*, functions as a target of miR168a as a major downstream effector of the miR168a pathway to be involved in both spike morphology and disease resistance. This is consistent with the OE168 phenotype, as the *ago1b* mutant also displayed increased susceptibility to and accelerated invasive progression of FHB, along with reduced spike length. We conclude here that the miR168a–*TaAGO1b* module influences multiple aspects of wheat plant development.

Previous studies showed that miR156 is involved in various plant activities, including integration of vegetative and reproductive growth, as well as plant structure (Bhogale et al., 2014; Chen et al., 2015; Wang et al., 2015; Miao et al., 2019). Normally, miR156 affects plant development by controlling the expression of *SQUAMOSA PROMOTER BINDING PROTEIN* (*SBP*)-*LIKE* (*SPL*) genes (Vaucheret et al., 2004; Liu et al., 2026). *TaSPL17* positively regulates grain size and number by regulating spikelet and floret meristem development, which leads to enhanced grain yield per plant (Liu et al., 2023). *TaSPL17* is one of the targets of miR156. Although 5′-RLM-RACE analysis supports miR156-mediated cleavage of *TaSPL17* transcripts, the relatively limited cleavage frequency suggests that transcript cleavage may not fully account for this regulation. It is reported that a subset of plant miRNAs can regulate their targets via transcript cleavage, translational repression, or both in rice (Rong et al., 2026). Therefore, we cannot exclude the possibility that translational repression or both contribute to miR156-mediated regulation of *TaSPL17* in wheat, which warrants further investigation. Despite this, the amount of miR156 was reduced in MIM168 lines, leading to overaccumulation of *SPL17*, whereas *TaSPL17* overexpression lines showed increased spike length and GNS (Liu et al., 2023). Conversely, *TaSPL17* knockout lines display decreased grain number per spike and grain number. In rice, miR168 modulates yield by increasing panicle number through miR535, representing a distinguishable regulatory pathway between wheat and rice.

miR444 is a monocot-specific miRNA family regulating plant growth, development, and stress responses by targeting MADS-box transcription factors, essentially acting as a crucial switch in complex signaling pathways in plants (Sunkar et al., 2005; Wu et al., 2009; Wang et al., 2016; Feng et al., 2023). Particularly, miR444b.2 responds to ambient temperature changes and modulates *HsfA1* transcript levels, thereby regulating rice blast disease (Qiu et al., 2025). In rice, miR168 regulates miR1320 and miR164 to participate in blast disease immunity (Wang et al., 2021). In our investigation, we identified miR444 to play a role in immunity against FHB. MIM444 transgenic plants exhibited fewer diseased spikelets and lower fungal biomass following spike inoculation, demonstrating that miR444 negatively regulates FHB resistance in wheat. Taken together, we propose a working model for the miR168a–*TaAGO1b* module as in Figure 7.

The miR168–*AGO1b* module plays a central role in maintaining small RNA homeostasis in wheat. As a core component of miRNA effector complexes, TaAGO1b abundance influences miRNA loading, stability, and activity, and can also regulate miRNA biogenesis through feedback mechanisms. In *ago1b* mutants, both mature miR156 and miR444 and their precursor transcripts accumulated to higher levels than in wild-type plants. This concomitant increase indicates that the effect of *TaAGO1b* occurs at or upstream of precursor accumulation, rather than simply through altered mature miRNA turnover, although further biochemical and genetic dissection is required to resolve the precise mechanism.

In rice, suppression of miR168 enhances yield, alters flowering time, and improves immunity by AGO1-mediated reshaping of downstream miRNA pathways, including miR535-associated yield regulation and miR1320/miR164-associated immune responses. In comparison, the downstream pathways connected to the wheat miR168–*TaAGO1b* module differ markedly. The miR156-*TaSPL17* pathway is tightly linked to spikelet meristem development and grain number, whereas miR444 is associated with *Fusarium* head blight (FHB) resistance. These distinctions point to functional specialization among *AGO1* homologs and reflect the different pathogen contexts examined in the two systems. Together, our findings underscore that the miR168–*AGO1* module serves as a conserved regulatory hub, but its downstream outputs are rewired in a species-specific manner to coordinate development and stress adaptation.

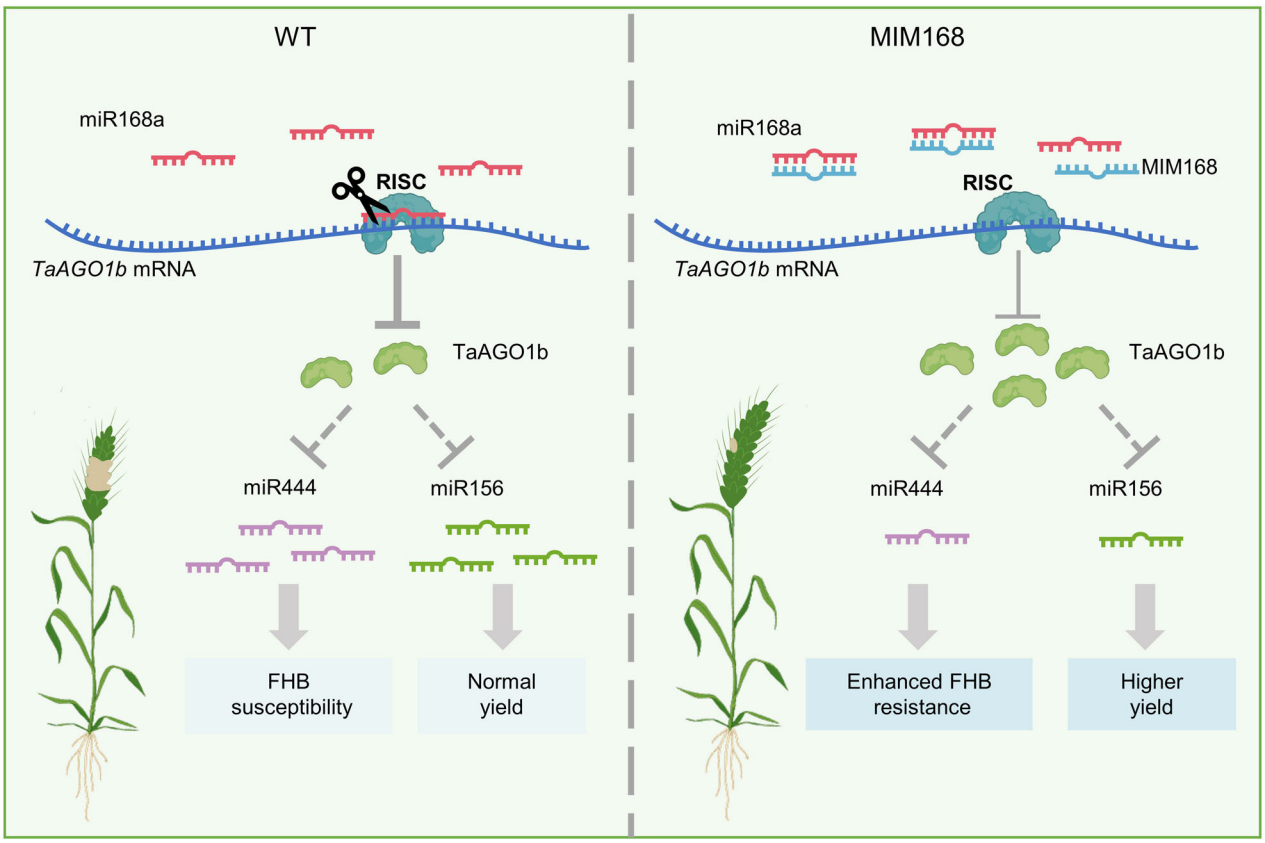

Figure 7. A working model for the miR168a–*TaAGO1b* module to breed high-yield and FHB-resistant wheat varieties
Left, miR168a guides the cleavage of *TaAGO1b* mRNA in WT, thereby decreasing TaAGO1b protein abundance. Right, in MIM168 plants, the decoy effect of MIM168 sequesters miR168a and prevents the degradation of *TaAGO1b* mRNA, leading to an increase in *TaAGO1b* abundance. Elevated TaAGO1b subsequently represses the levels of miR444 and miR156. This regulatory shift enhances FHB resistance and increases yield, demonstrating that manipulating the miR168a–*TaAGO1b* module is an effective strategy for breeding disease-resistant and high-yielding wheat. RISC: RNA-induced silencing complex.

Previous studies have identified key pathways involved in plant responses to *Fusarium* species, highlighting the combined use of structural and chemical defenses, including the action of effector proteins, toxin production, and phytohormone signaling (jasmonic acid, salicylic acid) (Dean et al., 2012). These signaling pathways play a crucial role in activating defense-related genes, which leads to enhanced synthesis of antimicrobial compounds and reinforcement of cellular barriers (Guerreiro and Marhavý, 2023). Building on this foundation, our research reveals specific functions of sRNAs in regulating resistance to FHB and delineates their complex regulatory networks controlling host defense responses. This insight not only deepens our understanding of plant–pathogen interactions but also offers promising avenues for engineering crop varieties with improved resistance through targeted manipulation of sRNA-mediated pathways.

We conclude that miR168a plays a dual role in disease resistance and yield enhancement. It promotes wheat development at the spikelet meristem stage, and upon pathogen attack it further defends against invasion at anthesis. Given that miR168a can regulate ROS homeostasis to enhance FHB resistance in wheat, future research will focus on functionally characterizing these mechanisms to identify novel regulators of wheat immunity and deepen our understanding of miRNA-mediated defense networks. Notably, under artificial inoculation conditions, MIM168 lines exhibited reduced yield loss, indicating improved yield stability under disease pressure. Future work will aim to introduce this regulatory module into elite cultivars to evaluate its potential for practical applications. The miR168a–*TaAGO1b* module provides evidence that enhancement of yield and disease resistance is achievable, highlighting a potential to breed high-yield, FHB-resistant wheat varieties in the future.

MATERIALS AND METHODS

Plant materials and growth conditions

The wheat cultivar Fielder was used as the wild-type (WT) background in this study. For phenotype analysis, plants were grown in a controlled greenhouse under a 22°C/16 h light and 18°C/8 h dark photoperiod. Wheat plants were cultivated in pots, with five plants per pot. For agronomic trait measurements, only the main spike of each plant was

analyzed to ensure consistency. For *F. graminearum* inoculation, only the main spike of each plant was inoculated, and disease severity was assessed by counting the number of diseased spikelets per spike.

For yield evaluation and the field-based FHB assay, WT and transgenic lines were cultivated at an experimental station in Shunyi, Beijing, China, during the 2025 and 2026 spring seasons. A randomized plot design with three independent biological replicates was used. Each replicate consisted of one plot containing 10 rows, with a row length of 2 m, 30 plants per row, and a row spacing of 30 cm, following local agronomic practices for spring wheat. All plants were managed using conventional irrigation and fertilization. Yield traits were evaluated under normal field conditions without pathogen inoculation. Field-based FHB assays were conducted in separate plots, where inoculation was performed using the same procedures as in greenhouse experiments, and disease severity was assessed by counting the number of diseased spikelets per spike.

Development of transgenic wheat plants

To generate the OE168 construct, a fragment containing the miR168a precursor together with approximately 300 bp of upstream and downstream flanking sequences was amplified from Fielder genomic DNA using specific primers (Table S1). The PCR product was cloned into the *Bam*HI/*Sac*I sites of the *pCAMBIA110* vector. To generate a target mimic (MIM168) construct, the target mimic sequence described in previous studies (Franco-Zorrilla et al., 2007) was synthesized and similarly inserted into the *Bam*HI/*Sac*I sites of the *pCAMBIA110* vector. To generate miR444-silenced transgenic plants, an STTM-based target mimic fragment containing two imperfect miR444 target sites separated by a 48 bp spacer was synthesized and cloned into the *pCAMBIA110* vector. To generate *TaAGO1b* and *TaAGO1c* knockout constructs, a gRNA targeting conserved regions of the three homoeologous copies was designed (Figure S7) and cloned into the *Bsa*I site of the *pHUE411* CRISPR/Cas9 vector. All transgenic materials, including miR168a overexpression lines (OE168) and miR168a knockdown lines (MIM168), miR444 knockdown plants (MIM444), as well as *TaAGO1b* and *TaAGO1c* gene-edited mutants, were generated in the Fielder background with *Agrobacterium*-mediated transformation (Ishida et al., 2015).

RT-qPCR and stem-loop RT-qPCR

Total RNA was extracted from wheat leaves and spikelets using TRIzol reagent (Thermo Fisher Scientific). For mRNA quantification, 1 μg of total RNA was reverse-transcribed using the PrimeScript RT reagent kit (Takara) (Jia et al., 2021). miRNA reverse transcription was performed with miRNA-specific stem-loop RT primers using the same kit. RT-qPCR was conducted with TB Green Premix Ex Taq (Takara) on the Applied Biosystems Step One Real-Time PCR system. miRNA quantification was carried out using a miRNA-specific forward primer together with a universal reverse primer (Feng et al., 2023). *GAPDH* and U6 snRNA served as internal reference genes for mRNA and miRNA assays, respectively. Relative expression levels were calculated using the $2^{-\Delta\Delta Ct}$ method (Jia et al., 2021). Each experiment included three biological replicates, and RT-qPCR reactions were performed with three technical replicates.

Pathogen infection and microscopy analysis

F. graminearum strain PH-1 and the GFP-tagged PH-1 derivative were used for disease assays. The strains were cultured on PDA plates at 28°C for 7 d (d), after which 6 mm mycelial plugs were transferred into mung bean broth and shaken at 28°C, 200 rpm for 3–5 d to induce conidiation (Bai et al., 2002). Conidia were harvested and suspended in sterile water containing 0.5% Tween-20, and the concentration was adjusted to 1×10^5 conidia mL^{-1}. At anthesis, 10 μL of the conidial suspension was applied to individual spikelets using the single-floret point-inoculation method, and spikes were covered with plastic bags for 24 h (h) to maintain humidity. The number of diseased spikelets (NDS) was recorded at 14 dpi. Disease severity was assessed by counting the number of diseased spikelets per spike in 30 independent spikes, providing robust support for the stability of the resistance phenotype under field conditions.

For the coleoptile infection assay, wheat seeds were germinated on moist filter paper for 3 d. When coleoptiles reached approximately 1.0–1.5 cm in length, the apical tip was excised to create a standardized wound, and 2.5 μL of the previously described conidial suspension was applied directly onto the cut surface (Wei et al., 2025). Inoculated seedlings were kept under high-humidity conditions for 24 h to facilitate infection.

F. graminearum was used for microscopic examination of fungal colonization in coleoptile tissues, and hyphal growth at 24 and 72 hpi was monitored using a confocal laser scanning microscope. Seedlings were then maintained under normal growth conditions, and lesion length was recorded at 5 dpi as a measure of disease severity.

Fungal biomass determination

To evaluate the fungal biomass of *F. graminearum* in wheat, infected spikelets were collected. Genomic DNA was extracted from approximately 100 mg of ground spikelet tissue using a CTAB-based method. Fungal biomass was quantified by qPCR using the *F. graminearum*-specific *Actin* gene and the wheat *TaActin* gene as internal references. The relative fungal biomass was calculated as the ratio of fungal DNA to wheat DNA using the $2^{-\Delta\Delta Ct}$ method. Each sample included three independent biological replicates.

Determination of DON content

DON content in infected wheat grains was quantified using a commercial deoxynivalenol ELISA kit (Solarbio, SEKSM-0007, Beijing, China) according to the manufacturer's instructions. Briefly, grain samples were ground, passed through a 20-mesh sieve, and extracted with deionized water. After centrifugation, the supernatant was diluted as recommended

by the manufacturer and used for ELISA detection. Absorbance was measured at 450 nm with 630 nm as the reference wavelength. The relative absorbance percentage was calculated by normalization to the zero standard, and DON concentrations were determined using a four-parameter logistic standard curve. Final DON content was corrected using the dilution factor of 20 and expressed as ppm.

H_2O_2 accumulation analysis

To detect hydrogen peroxide (H_2O_2) accumulation in wheat after *F. graminearum* infection, 3,3′-diaminobenzidine (DAB) staining was performed. Leaf samples were collected at the indicated time points after inoculation, vacuum-infiltrated with DAB solution (1 mg mL^{-1}, pH 3.6), and incubated in the dark at room temperature overnight. After staining, chlorophyll was removed using ethanol/acetic acid (3:1, v/v), and samples were cleared before imaging.

For quantitative measurement, H_2O_2 content in infected spikelets was determined using an H_2O_2 Assay Kit (Solarbio, BC3595) according to the manufacturer's instructions. Briefly, ~0.1 g of tissue was homogenized in acetone, and the resulting extracts were used for colorimetric detection based on the formation of a titanium–peroxide complex. Absorbance was measured at 415 nm, and H_2O_2 content was expressed as μmol g^{-1} fresh weight. Each treatment included at least three independent biological replicates.

Quantification of GFP-positive fungal area

For quantification of fungal colonization, microscopic images of infected wheat coleoptiles were analyzed using ImageJ software. The GFP channel was used to identify fungal hyphae. The GFP-positive hyphal region was selected by applying the same threshold settings to all images within the same experiment. The total observed coleoptile tissue area in each image was defined as the region of interest, excluding non-tissue background and scale bars. Fungal colonization was calculated as the percentage of GFP-positive fungal area relative to the total observed coleoptile tissue area and is presented as GFP-positive fungal area (%).

BSMV (barley stripe mosaic virus)-mediated miRNA silencing

BSMV-mediated silencing of endogenous miR444 (miR444b.1:UGUUGUCUCAAGCUUGCUGCC) was achieved using a short tandem target mimic (STTM) strategy as described previously. The STTM444 construct contained two tandem miR444 target sites separated by a 48 bp linker sequence. The STTM fragment was synthesized commercially (Sangon Biotech) and cloned into the *Nde*I site of the BSMV:γ vector. At the two-leaf stage of wheat cultivar Fielder, equal volumes of BSMV:α, BSMV:β, and BSMV:γ were mixed and mechanically inoculated onto the second leaf (Holzberg et al., 2002). Plants were misted with DEPC-treated water and kept under high-humidity conditions for 24 h. When the positive control BSMV:*PDS* exhibited characteristic photobleaching symptoms, the fourth leaf was collected to quantify miR444 expression. For disease assays, the fourth leaf was placed on agar plates and gently wounded with a scalpel, followed by inoculation with 2.5 μL of the *F. graminearum* conidial suspension. Inoculated leaves were incubated under standard conditions, and lesion length was recorded at 5 dpi to evaluate the impact of miR444 silencing on FHB resistance.

5′-RLM-RACE assays

5′ RNA ligase-mediated rapid amplification of cDNA ends (5′-RLM-RACE) was performed as previously described with minor modifications (Neller et al., 2019). Briefly, 250 ng of poly (A) mRNA was ligated to 250 ng of a 5′ RNA adapter using T4 RNA ligase (NEB) at 37°C for 1 h. The ligation products were purified and reverse-transcribed into cDNA using the PrimeScript RT reagent kit (Takara). Based on the predicted miRNA cleavage site on target mRNA, outer and inner gene-specific primers were designed approximately 150–300 bp downstream of the cleavage position. A two-step nested PCR was performed using the outer primers for the first amplification and the inner primers for the second amplification to obtain specific RACE fragments. The resulting PCR products were gel-purified, cloned into the pGEM-T Easy vector (Promega), and transformed into *E. coli* DH5α competent cells. Individual colonies were sequenced to determine the precise miRNA cleavage site.

Luciferase imaging assays

To assess the effects of miR168a on *TaAGO1b* and *TaAGO1c*, equal concentrations and volumes of *Agrobacterium* GV3101 harboring the indicated WT and mutated target site of *TaAGO1b* or *TaAGO1c* along with pre-miR168a were co-infiltrated into *Nicotiana benthamiana* leaves. At least four leaves from independent *N. benthamiana* plants were infiltrated, and the fluorescence signal was observed. For observation of the fluorescence signal, the injected tobacco leaves were kept in dark conditions for 5 min after a spray of Luciferin (100 μM). The LUC images were taken by the imaging device (Tanon 5200), and the LUC signals were measured by the Dual Luciferase Reporter Gene Assay Kit (Coolaber, China) and calculated as the LUC/REN ratio.

RNA-seq and small RNA-seq analysis

Total RNA was extracted from wheat spikelets at 48 hpi with mock or *F. graminearum*, as well as from young spikes at the W3.5 developmental stage, using TRIzol reagent (Thermo Fisher Scientific). RNA-seq libraries were constructed and sequenced on the Illumina NovaSeq platform to generate 150 bp paired-end reads. Transcriptome reads were aligned to the IWGSC RefSeq v1.1 wheat genome using HISAT2 (v2.0.5), and gene-level counts were obtained with featureCounts (v2.0.1). Differential expression analysis was performed using DESeq2 with thresholds of P-adjust < 0.05 and $|Log_2FC| > 1$, followed by GO and KEGG enrichment analyses using clusterProfiler. Global transcriptome variation was assessed by principal component analysis and sample-to-sample Pearson correlation (Guan et al., 2022).

For small RNA-seq, libraries were generated by ligating 3′ and 5′ adapters to total RNA, synthesizing first-strand cDNA, and PCR-enriching fragments of 18–40 nt, followed by size selection and sequencing on an Illumina platform. Raw reads were filtered using fastp to remove adapter contamination, poly-N reads, and low-quality reads, and sequencing quality (Q20/Q30/GC content) was evaluated. High-quality small RNA reads were aligned to the IWGSC RefSeq v1.1 genome using Bowtie. Known miRNAs were identified using miRBase annotations combined with miRDeep2, and novel miRNAs were predicted using miREvo and miRDeep2 based on precursor hairpin structure, Dicer cleavage signatures, and minimal free energy. miRNA expression levels were normalized to TPM, and differential expression analysis was performed using DESeq2. Target genes of known and predicted miRNAs were identified using psRobot (Dai and Zhao, 2011).

Statistical analysis

Data were compiled and analyzed using Microsoft Excel 2021 and GraphPad Prism 9.5. Statistical significance was determined using two-tailed Student's *t*-tests, or one-way ANOVA followed by Dunnett's multiple comparisons test, as indicated in the Figure legends. All values are means ± *SD* and three independent biological replicates were performed.

Generative AI usage statement

During the preparation of this work, ChatGPT was employed by the authors for language editing and polishing. After utilizing ChatGPT, the authors conducted a careful review and, where necessary, revised the content, and took full responsibility for the final version of the publication.

Data availability statement

The sequencing data have been deposited in the Genome Sequence Archive in the National Genomics Data Center, China National Center for Bioinformation/Beijing Institute of Genomics, Chinese Academy of Sciences (under Accession PRJCA057223, PRJCA057224, PRJCA057225, and PRJCA057226) that are publicly accessible at Genome Sequence Archive -CNCB-NGDC.

ACKNOWLEDGEMENTS

This research was supported by Key R&D Program of Shandong Province, China (Grant No.2024SFGC0404), the Innovation Program of Chinese Academy of Agricultural Sciences (CAAS-ZDRW202403), the National Natural Science Foundation of China (3257151902, 32201878, 32172050, and W2411025), the Hebei Natural Science Foundation (C2025205068). We gratefully acknowledge the technical assistance provided by the Key Facility Center of ICS, CAAS, for RNA-seq library preparation and sequencing.

CONFLICTS OF INTEREST

The authors declare no conflicts of interest.

AUTHOR CONTRIBUTIONS

L.M., A.L., S.L., and M.Z. designed the research, analyzed the data, and supervised the project. G.C., S.G., and Z.D. created genetic populations and materials. G.C., Z.D., T.C., and S.L. performed experiments. Y.C. and Z.W. performed the small RNA-seq and transcriptome analysis. Q.C., D.C., X.Z., W.X., Z.Z., Z.Y., T.L., and Z.Y. performed the field tests in Beijing. X.L., J.W., S.G., M.Z., A.L., L.M., and S.L. drafted and edited the manuscript. All authors have read and approved the contents of this paper.

Edited by: Yijun Qi, Tsinghua University, China

Received Apr. 9, 2026; **Accepted** Aug. 26, 2026

REFERENCES

Alisaac, E., and Mahlein, A.K. (2023). *Fusarium* head blight on wheat: Biology, modern detection and diagnosis and integrated disease management. Toxins (Basel) **15:** 192.

Annacondia, M.L., and Martinez, G. (2021). Reprogramming of RNA silencing triggered by cucumber mosaic virus infection in Arabidopsis. Genome Biol. **22:** 340.

Attallah, C., Conti, G., Zuljan, F., Zavallo, D., and Ariel, F. (2025). Noncoding RNAs as tools for advancing translational biology in plants. Plant Cell **37:** koaf054.

Bai, G.-H., Desjardins, A., and Plattner, R. (2002). Deoxynivalenol-nonproducing *Fusarium graminearum* causes initial infection, but does not cause disease spread in wheat spikes. Mycopathologia **153:** 91–98.

Bhogale, S., Mahajan, A.S., Natarajan, B., Rajabhoj, M., Thulasiram, H.V., and Banerjee, A.K. (2014). MicroRNA156: A potential graft-transmissible microRNA that modulates plant architecture and tuberization in *Solanum tuberosum* ssp. *andigena*. Plant Physiol. **164:** 1011–1027.

Carbonell, A. (2017). Plant ARGONAUTEs: Features, functions, and unknowns. Methods Mol. Biol. **1640:** 1–21.

Chen, X. (2009). Small RNAs and their roles in plant development. Annu. Rev. Cell Dev. Biol. **25:** 21–44.

Chen, Z., Gao, X., and Zhang, J. (2015). Alteration of osa-miR156e expression affects rice plant architecture and strigolactones (SLs) pathway. Plant Cell Rep. **34:** 767–781.

Dai, X., and Zhao, P.X. (2011). psRNATarget: A plant small RNA target analysis server. Nucleic Acids Res. **39:** W155–W159.

Dean, R., Van Kan, J.A.L., Pretorius, Z.A., Hammond-Kosack, K.E., Di Pietro, A., Spanu, P.D., Rudd, J.J., Dickman, M., Kahmann, R., Ellis, J., et al. (2012). The Top 10 fungal pathogens in molecular plant pathology. Mol. Plant Pathol. **13:** 414–430.

Fahad, M., Tariq, L., Li, W., and Wu, L. (2025). MicroRNA gatekeepers: Orchestrating rhizospheric dynamics. J. Integr. Plant Biol. **67:** 845–876.

Feng, T., Zhang, Z.-Y., Gao, P., Feng, Z.-M., Zuo, S.-M., and Ouyang, S.-Q. (2023). Suppression of rice Osa-miR444.2 improves the resistance to sheath blight in rice mediating through the phytohormone pathway. Int. J. Mol. Sci. **24:** 3653.

Franco-Zorrilla, J.M., Valli, A., Todesco, M., Mateos, I., Puga, M.I., Rubio-Somoza, I., Leyva, A., Weigel, D., García, J.A., and Paz-Ares, J. (2007). Target mimicry provides a new mechanism for regulation of microRNA activity. Nat. Genet. **39:** 1033–1037.

Guan, J., Wang, Z., Liu, S., Kong, X., Wang, F., Sun, G., Geng, S., Mao, L., Zhou, P., and Li, A. (2022). Transcriptome analysis of developing

wheat grains at rapid expanding phase reveals dynamic gene expression patterns. Biology **11:** 281.

Guerreiro, J., and Marhavý, P. (2023). Unveiling the intricate mechanisms of plant defense. Front. Plant Physiol. **1:** 1285373.

Guo, J., Zhang, T., Xie, H., Hu, H., Shi, C., Zhao, Y., Yin, J., Xu, G., Wu, Z., Wang, P., et al. (2025). An m6A methyltransferase confers host resistance by degrading viral proteins through ubiquitination. Nat. Commun. **16:** 4821.

Guo, M., Liu, S., Pan, Y., Huang, Y., Kong, L., Zhang, Y., Liu, H., Hou, J., Liu, H., Zhang, X., et al. (2026). The miR171a-*TaSCL6-1* module acts downstream of miR164-targeted *TaNAC21/22* to regulate leaf rust resistance in wheat. Plant Biotechnol. J. **24:** 3723–3738.

He, Z., Webster, S., and He, S.Y. (2022). Growth-defense trade-offs in plants. Curr. Biol. **32:** R634–r639.

Holzberg, S., Brosio, P., Gross, C., and Pogue, G.P. (2002). Barley stripe mosaic virus-induced gene silencing in a monocot plant. Plant J. **30:** 315–327.

Iki, T., Cléry, A., Bologna, N.G., Sarazin, A., Brosnan, C.A., Pumplin, N., Allain, F.H.T., and Voinnet, O. (2018). Structural flexibility enables alternative maturation, ARGONAUTE sorting and activities of miR168, a global gene silencing regulator in plants. Mol. Plant **11:** 1008–1023.

Ishida, Y., Tsunashima, M., Hiei, Y., and Komari, T. (2015). Wheat (*Triticum aestivum* L.) transformation using immature embryos. Methods Mol. Biol. **1223:** 189–198.

Jia, M., Li, Y., Wang, Z., Tao, S., Sun, G., Kong, X., Wang, K., Ye, X., Liu, S., Geng, S., et al. (2021). TaIAA21 represses TaARF25-mediated expression of *TaERFs* required for grain size and weight development in wheat. Plant J. **108:** 1754–1767.

Kapoor, M., Arora, R., Lama, T., Nijhawan, A., Khurana, J.P., Tyagi, A.K., and Kapoor, S. (2008). Genome-wide identification, organization and phylogenetic analysis of Dicer-like, Argonaute and RNA-dependent RNA Polymerase gene families and their expression analysis during reproductive development and stress in rice. BMC Genomics **9:** 451.

Karasov, T.L., Chae, E., Herman, J.J., and Bergelson, J. (2017). Mechanisms to mitigate the trade-off between growth and defense. Plant Cell **29:** 666–680.

Li, G., Yuan, Y., Zhou, J., Cheng, R., Chen, R., Luo, X., Shi, J., Wang, H., Xu, B., Duan, Y., et al. (2023). FHB resistance conferred by Fhb1 is under inhibitory regulation of two genetic loci in wheat (*Triticum aestivum* L.). Theor. Appl. Genet. **136:** 134.

Li, G., Zhou, J., Jia, H., Gao, Z., Fan, M., Luo, Y., Zhao, P., Xue, S., Li, N., Yuan, Y., et al. (2019). Mutation of a histidine-rich calcium-binding-protein gene in wheat confers resistance to Fusarium head blight. Nat. Genet. **51:** 1106–1112.

Li, S., Lin, D., Zhang, Y., Deng, M., Chen, Y., Lv, B., Li, B., Lei, Y., Wang, Y., Zhao, L., et al. (2022a). Genome-edited powdery mildew resistance in wheat without growth penalties. Nature **602:** 455–460.

Li, Z., Li, W., Guo, M., Liu, S., Liu, L., Yu, Y., Mo, B., Chen, X., and Gao, L. (2022b). Origin, evolution and diversification of plant ARGONAUTE proteins. Plant J. **109:** 1086–1097.

Liu, Q., Zhang, L., Zhou, Z., Zhang, C., Li, C., Debernardi, J.M., and Dubcovsky, J. (2026). MicroRNA156 and its targeted *SPL* genes interact with the photoperiod, vernalization, and gibberellin pathways to regulate wheat heading time. Plant J. **125:** e70656.

Liu, S., Dai, J., Huang, J., Wen, Z., Zhang, W., Shen, L., Jackson, R., Wang, X.e, Deakin, G., Xiao, J., et al. (2025). Combining ultralow-altitude drone phenotyping with deep learning analytics to assess resistance and disease dynamics of Fusarium head blight in wheat. Crop J. **13:** 1372–1385.

Liu, S., Zhang, F., Su, J., Fang, A., Tian, B., Yu, Y., Bi, C., Ma, D., Xiao, S., and Yang, Y. (2024). CRISPR-targeted mutagenesis of mitogen-activated protein kinase phosphatase 1 improves both immunity and yield in wheat. Plant Biotechnol. J. **22:** 1929–1941.

Liu, X., Tan, C., Cheng, X., Zhao, X., Li, T., and Jiang, J. (2020). miR168 targets Argonaute1A mediated miRNAs regulation pathways in response to potassium deficiency stress in tomato. BMC Plant Biol. **20:** 477.

Liu, Y., Chen, J., Yin, C., Wang, Z., Wu, H., Shen, K., Zhang, Z., Kang, L., Xu, S., Bi, A., et al. (2023). A high-resolution genotype–phenotype map identifies the *TaSPL17* controlling grain number and size in wheat. Genome Biol. **24:** 196.

Lopez-Gomollon, S., and Baulcombe, D.C. (2022). Roles of RNA silencing in viral and non-viral plant immunity and in the crosstalk between disease resistance systems. Nat. Rev. Mol. Cell Biol. **23:** 645–662.

Lu, K., Chen, X., Yao, X., An, Y., Wang, X., Qin, L., Li, X., Wang, Z., Liu, S., Sun, Z., et al. (2022). Phosphorylation of a wheat aquaporin at two sites enhances both plant growth and defense. Mol. Plant **15:** 1772–1789.

Miao, C., Wang, Z., Zhang, L., Yao, J., Hua, K., Liu, X., Shi, H., and Zhu, J.-K. (2019). The grain yield modulator miR156 regulates seed dormancy through the gibberellin pathway in rice. Nat. Commun. **10:** 3822.

Morel, J.B., Godon, C., Mourrain, P., Béclin, C., Boutet, S., Feuerbach, F., Proux, F., and Vaucheret, H. (2002). Fertile hypomorphic *ARGONAUTE* (*ago1*) mutants impaired in post-transcriptional gene silencing and virus resistance. Plant Cell **14:** 629–639.

Neller, K.C., Klenov, A., and Hudak, K.A. (2019). Prediction and characterization of miRNA/target pairs in non-model plants using RNA-seq. Curr. Protoc. Plant Biol. **4:** e20090.

Ning, Q., Ding, F., Jia, M., Zhang, Y., Liu, Y., Yang, W., Lyu, Z., Cai, Y., Zhu, Z., Liu, Y., et al. (2026). Allelic variation at *TaMYB30-B1* is associated with enhanced Fusarium head blight resistance in wheat lacking *Fhb1*. Crop J. **14:** 1064–1071.

Qiu, J., Cao, X., Shi, H., Chen, Z., Zhang, X., Cao, Z., Huang, D., Wen, H., Chen, Y., and Kou, Y. (2025). *miR444b.2–HsfA1–AOC1* module mediates heat priming-enhanced blast resistance in rice. Proc. Natl. Acad. Sci. U. S. A. **122:** e2505764122.

Rong, F., Zhang, Y., Ni, F., Zhang, L., Yu, M., Hong, Z., Fahad, M., Shen, Y., Liu, C., Tian, S., et al. (2026). miR408-5p and miR408-3p cooperatively reduce cadmium uptake and accumulation in rice. PLoS Biol. **24:** e3003811.

Shang, S., He, Y., Hu, Q., Fang, Y., Cheng, S., and Zhang, C.J. (2024). *Fusarium graminearum* effector FgEC1 targets wheat TaGF14b protein to suppress TaRBOHD-mediated ROS production and promote infection. J. Integr. Plant Biol. **66:** 2288–2303.

Shen, E., Zhao, T., and Zhu, Q.-H. (2024). Are miRNAs applicable for balancing crop growth and defense trade-off? New Phytol. **243:** 1670–1680.

Song, R., Zhang, D., Yang, J., Cheng, Y., Song, X., Zhao, W., Xia, M., Zhang, Y., Wei, L., Cheng, M., et al. (2024). Identification and transferring of a new Fusarium head blight resistance gene *FhbRc2* from *Roegneria ciliaris* 3ScL chromosome arm into common wheat. Crop J. **12:** 1718–1726.

Su, Z., Bernardo, A., Tian, B., Chen, H., Wang, S., Ma, H., Cai, S., Liu, D., Zhang, D., Li, T., et al. (2019). A deletion mutation in *TaHRC* confers *Fhb1* resistance to Fusarium head blight in wheat. Nat. Genet. **51:** 1099–1105.

Sunkar, R., Girke, T., Jain, P.K., and Zhu, J.K. (2005). Cloning and characterization of microRNAs from rice. Plant Cell **17:** 1397–1411.

Tang, J., and Chu, C. (2017). MicroRNAs in crop improvement: Fine-tuners for complex traits. Nat. Plants **3:** 17077.

Várallyay, E., Válóczi, A., Agyi, A., Burgyán, J., and Havelda, Z. (2010). Plant virus-mediated induction of miR168 is associated with repression of ARGONAUTE1 accumulation. EMBO J. **29:** 3507–3519.

Vaucheret, H., Mallory, A.C., and Bartel, D.P. (2006). AGO1 homeostasis entails coexpression of MIR168 and *AGO1* and preferential stabilization of miR168 by AGO1. Mol. Cell **22:** 129–136.

Vaucheret, H., Vazquez, F., Crété, P., and Bartel, D.P. (2004). The action of ARGONAUTE1 in the miRNA pathway and its regulation by the miRNA pathway are crucial for plant development. Genes Dev. **18:** 1187–1197.

Viviani, A., Haile, J.K., Fernando, W.G.D., Ceoloni, C., Kuzmanović, L., Lhamo, D., Gu, Y.Q., Xu, S.S., Cai, X., Buerstmayr, H., et al. (2025). Priority actions for Fusarium head blight resistance in durum wheat: Insights from the wheat initiative. Plant Genome **18:** e20539.

Waddington, S., Cartwright, P., and Wall, P. (1983). A quantitative scale of spike initial and pistil development in barley and wheat. Ann. Bot. **51:** 119–130.

Wang, H., Jiao, X., Kong, X., Hamera, S., Wu, Y., Chen, X., Fang, R., and Yan, Y. (2016). A signaling cascade from miR444 to RDR1 in rice antiviral RNA silencing pathway. Plant Physiol. **170:** 2365–2377.

Wang, H., Li, Y., Chern, M., Zhu, Y., Zhang, L.-L., Lu, J.-H., Li, X.-P., Dang, W.-Q., Ma, X.-C., Yang, Z.-R., et al. (2021). Suppression of rice miR168 improves yield, flowering time and immunity. Nat. Plants **7:** 129–136.

Wang, H., Sun, S., Ge, W., Zhao, L., Hou, B., Wang, K., Lyu, Z., Chen, L., Xu, S., Guo, J., et al. (2020). Horizontal gene transfer of *Fhb7* from fungus underlies *Fusarium* head blight resistance in wheat. Science **368:** eaba5435.

Wang, L., Sun, S., Jin, J., Fu, D., Yang, X., Weng, X., Xu, C., Li, X., Xiao, J., and Zhang, Q. (2015). Coordinated regulation of vegetative and reproductive branching in rice. Proc. Natl. Acad. Sci. U.S.A. **112:** 15504–15509.

Wei, W.-Q., Li, S., Zhang, D., and Tang, W.-H. (2025). Single-cell transcriptomic analysis highlights specific cell types manipulated by Fusarium head blight fungus leading to wheat susceptibility. Dev. Cell **60:** 3496–3513.e3496.

Wu, L., Zhang, Q., Zhou, H., Ni, F., Wu, X., and Qi, Y. (2009). Rice MicroRNA effector complexes and targets. Plant Cell **21:** 3421–3435.

Xian, Z., Huang, W., Yang, Y., Tang, N., Zhang, C., Ren, M., and Li, Z. (2014). miR168 influences phase transition, leaf epinasty, and fruit development via SlAGO1s in tomato. J. Exp. Bot. **65:** 6655–6666.

Yu, Y., Wang, H., You, C., and Chen, X. (2026). Plant microRNA maturation and function. Nat. Rev. Mol. Cell Biol. **27:** 55–70

Zhang, H., Xia, R., Meyers, B.C., and Walbot, V. (2015). Evolution, functions, and mysteries of plant ARGONAUTE proteins. Curr. Opin. Plant Biol. **27:** 84–90.

Zhao, S., Ren, J., Hu, Q., Dong, C., Lian, B., Liu, X., Wu, M., and Wu, J.-G. (2026). An AGO2–miR167g-3p–*SNAP32* module confers antiviral immunity in rice. J. Integr. Plant Biol. **68:** 812–827.

Zhao, Z.X., Yang, S.-J., Yin, X.-X., Yan, X.-L., Hassan, B., Fan, J., Li, Y., and Wang, W.-M. (2023). ARGONAUTE 1: A node coordinating plant disease resistance with growth and development. Phytopathol. Res **5:** 38.

Zhou, J., Zhang, R., Jia, X., Tang, X., Guo, Y., Yang, H., Zheng, X., Qian, Q., Qi, Y., and Zhang, Y. (2022). CRISPR-Cas9 mediated *OsMIR168a* knockout reveals its pleiotropy in rice. Plant Biotechnol. J. **20:** 310–322.

Zhou, Y., Zhou, S., Wang, L., Wu, D., Cheng, H., Du, X., Mao, D., Zhang, C., and Jiang, X. (2020). miR164c and miR168a regulate seed vigor in rice. J. Integr. Plant Biol. **62:** 470–486.

SUPPORTING INFORMATION

Additional Supporting Information may be found online in the supporting information tab for this article: http://onlinelibrary.wiley.com/doi/10.1111/jipb.70387/suppinfo

Figure S1. Predicted secondary structures of pre-miR168a homoeologs and infection-responsive expression of miR168a in wheat
Figure S2. Knockdown of miR168a increases spike length and grain number under greenhouse conditions
Figure S3. Spike length and grain phenotypes of WT, OE168, and MIM168 lines in the field
Figure S4. Structural features and tissue-specific expression patterns of *TaAGO1s* gene family members
Figure S5. Expression patterns of *TaAGO1b* homoeologs in miR168a transgenic plants and during *Fusarium graminearum* infection
Figure S6. Expression patterns of *TaAGO1c* in transgenic plants
Figure S7. CRISPR/Cas9-mediated generation of *TaAGO1b* and *TaAGO1c* mutants
Figure S8. Spike and grain phenotypes of *ago1b* and *ago1c* mutants
Figure S9. Co-expression clusters of miRNAs identified in W3.5-stage spikelets and validation of miR156 accumulation in *ago1b* mutants
Figure S10. Transcriptome dynamics of young spikes in Fielder, MIM168, and OE168 at the W3.5 stage
Figure S11. Transcriptomic responses of spikelets during *F. graminearum* infection and validation of miR444 accumulation in *ago1b* mutants
Figure S12. BSMV-mediated silencing of miR444 in wheat leaves
Table S1. Primers used in the study
Table S2. miRNA TPM values in Fielder, MIM168, and OE168 at the W3.5 stage
Table S3. Predicted target genes of miRNAs in spikelets at the W3.5 stage
Table S4. miRNA TPM values in Fielder, MIM168, and OE168 at 48 h post inoculation (hpi)
Table S5. Predicted target genes of miRNAs in response to *Fusarium graminearum* infection
Table S6. Gene accession IDs of wheat *AGO1* family members used in this study
Table S7. Genes associated with the GO term "oxalate oxidase activity" in MIM168-specific upregulated genes after infection